Simulation of Semiconductor Processes and Devices 2016
Edited by E. Bär, J. Lorenz, and P. Pichler

Electric Response of Ovonic Materials to Oscillating Potentials

E. Piccinini, R. Brunetti[1], M. Rudan, and C. Jacoboni[1]
DEI Department, University of Bologna, Via Risorgimento 2, I-40136, Bologna, Italy, massimo.rudan@unibo.it
[1]FIM Department, University of Modena and Reggio Emilia, Via Campi 213/A, I-41125 Modena, Italy

***Abstract*—This paper presents a computational analysis, by means of a compact model, of the electric response of an Ovonic Threshold-Switch device embedded in a circuit subjected to an oscillatory bias.**

I. Introduction

Ovonic threshold switch (OTS) and phase-change materials have been selected by some leading electronic industries as semiconductors for innovative devices in the field of data storage, and proposed for beyond-von Neumann calculators and bio-inspired neuromorphic computing. Recently, planar arrays of chalcogenide-based devices have been realized, and commercial mass production has been announced. This paper addresses the issue of the single OTS-device response to oscillating potentials.

The $I(V)$ curve of an Ovonic device exhibits two stable states featuring different resistivities, with a typical S-shaped current-voltage characteristic [1], [2], [3], [4], [5]. Most investigators agree in ascribing the above behavior to hot-carrier phenomena [6], [7]; according to this interpretation, different carrier temperatures are at the origin of the two resistivity states. It must be remarked that most of the electrical analyses published in the literature refer to steady-state conditions; only recently, experimental evidence pointed out that the transient features related, e.g., to how the bias is applied [8] or to the recovery time after the bias is changed [9], introduce new issues about the switching process. The new physical phenomena that appear in dynamic conditions are relevant for the design of high-speed devices when the switching dynamics becomes fast enough to couple significantly with the microscopic times intrinsic to the semiconductor, and/or with the characteristic times of the external circuitry.

II. Model

The analysis is based on the model of [10], [11], which assumes a trap-limited transport scheme. Two energy levels are available for the carriers, separated by an energy gap $\Delta E_0 = E_B - E_T > 0$. Electrons in the deep trap states E_T do not contribute to the electric current; those in the upper level E_B, which mimicks shallow trap states and band states, are mobile. The device is one dimensional and spatially uniform, and the total carrier concentration $n = n_B + n_T$ is fixed. The transport equations (1–3), whose unknowns are the concentration n_B

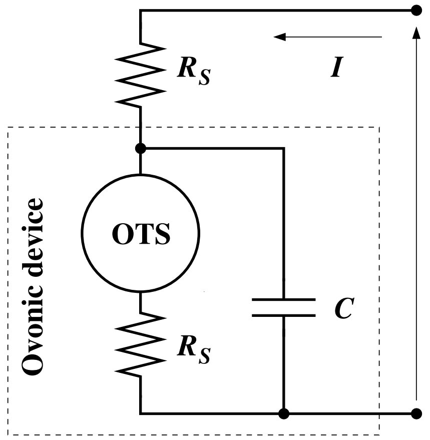

Fig. 1. The circuit investigated in the paper. The boxed area represents an Ovonic device including the active layer OTS and the parasitic effects; the latter are modeled by the two constants R_S and C.

and temperature T_e of the band electrons, are coupled to the circuit equation (4); they describe time-dependent situations with a limited computational load. The microscopic parameters appearing in the constitutive equations of the model are fixed through comparisons with existing steady-state and transient experimental data [11]. The model equations read

$$\tilde{n}_B = \frac{n}{1 + \Gamma \, \exp\left[(\Delta E_0 - \gamma\,|F|)/(k\,T_e)\right]}\,, \tag{1}$$

$$\frac{\mathrm{d}n_B}{\mathrm{d}t} = -\frac{n_B - \tilde{n}_B}{\tau_N}\,, \qquad J = q\,\mu\,n_B\,F\,, \tag{2}$$

$$\frac{\mathrm{d}\varepsilon}{\mathrm{d}t} = J\,F - n\,\frac{k\,T_e - k\,T_0}{\tau_T}\,, \tag{3}$$

$$\frac{\mathrm{d}I}{\mathrm{d}t} = \frac{V - F\,L + C\,R_S\,\mathrm{d}V/\mathrm{d}t - I\,(R_S + R_L)}{C\,R_S\,R_L}\,. \tag{4}$$

Eq. (1) provides the steady-state, non-equilibrium concentration of the band electrons; the term $\gamma\,|F|$ accounts for the traps' edge lowering due to Poole's effect [6], [7]. The first and second equations in (2) are the continuity and transport equation for the band electrons, respectively, while equation (3) is the continuity equation for the band-electron energy ε. Finally, (4) is the circuit's equation. The meaning of the other symbols in (1–4) is given in Tab. I and Fig. 1.

In the steady-state condition it is $n_B = \tilde{n}_B$. Also, using in the steady-state form of (3) the expression of J obtained from the

978-1-5090-0818-6/16/$31.00

second equation in (2), and defining the constant electric field $F_0 = \sqrt{k\,T_0/(q\,\mu\,\tau_T)}$, one finds

$$\frac{T_e}{T_0} = 1 + \frac{n_B}{n}\,\frac{F^2}{F_0^2}\,. \tag{5}$$

It follows that in steady state it is $T_e \geq T_0$. By the same token, one recasts (1) as $n/n_B = 1 + \Gamma\,\exp\,[(\Delta E_0 - \gamma\,|F|)/(k\,T_e)]$, to find that the steady-state limits of n_B are given by

$$1 < \frac{n}{n_B} \leq 1 + \Gamma\,\exp\left(\frac{\Delta E_0}{k\,T_0}\right). \tag{6}$$

In a one-dimensional, uniform material, the device voltage and current are given by $L\,F$, $A\,J$, with A the device's cross-sectional area. Thus, to find the steady-state characteristic of the Ovonic device it suffices to determine the relation between F and J. This is accomplished in parametric form, after inverting (1) and taking $k\,T_e$ from (5):

$$\frac{\Delta E_0 - \gamma\,|F|}{k\,T_0\,\log[(n/n_B - 1)/\Gamma]} = 1 + \frac{n_B}{n}\,\frac{F^2}{F_0^2}\,. \tag{7}$$

Solving (7) as a second-degree equation in $|F|$, one determines the $F(n_B)$ relation (being F spatially uniform, its sign is always determined). Then, by successively giving n_B all values fulfilling (6), one uses the relation just found to calculate F, while the value of J corresponding to it is given by $J = q\,\mu\,n_B\,F$. The steady-state $I(V)$ curve of Fig. 2 has been determined in this way.

III. Response to a Periodic Voltage

The low- and high-resistance states of an Ovonic device are important for controlling the access features to a phase-change memory bit in cross-point array architectures [12]. Thus, in view of the technological application it is necessary to assess the conductive state of the device. In this section we test the response of the Ovonic device in a circuit subjected to a periodic voltage. As expected, the device response depends on how the material's and circuit's characteristic times compare; also, depending on the frequency and amplitude of the applied voltage, different electric regimes may set in.

TABLE I

Model Parameters

n	Total electron concentration (band+traps)
Γ	Normalized density of states of the band
ΔE_0	Band-trap energy difference
F	Electric field
q	Absolute value of the electron charge
k	Boltzmann constant
T_e	Electron temperature
T_0	Equilibrium temperature
τ_N	Relaxation time of the band electrons
τ_T	Relaxation time of the band electrons' energy
μ	Mobility of the band electrons
J	Current density across the Ovonic device
γ	Poole's effect parameter
L	Length of the Ovonic device

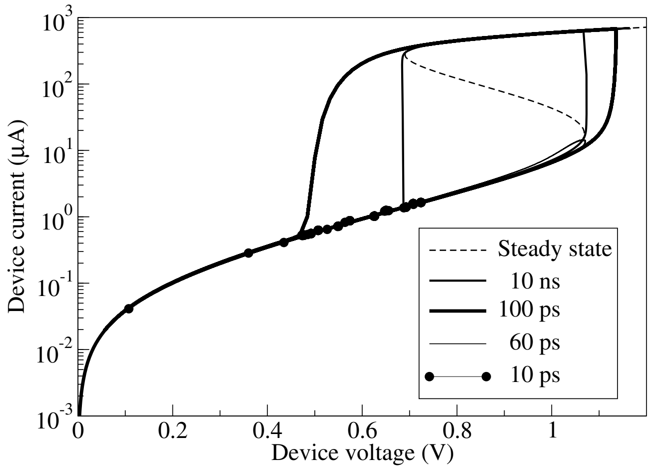

Fig. 2. Current response of the Ovonic device in the circuit of Fig. 1 to an applied voltage $V = (V_0/2)\,[1 - \cos(2\,\pi\,t/T)]$, with $V_0 = 1.2$ V and different periods T (the latter are shown in the legend).

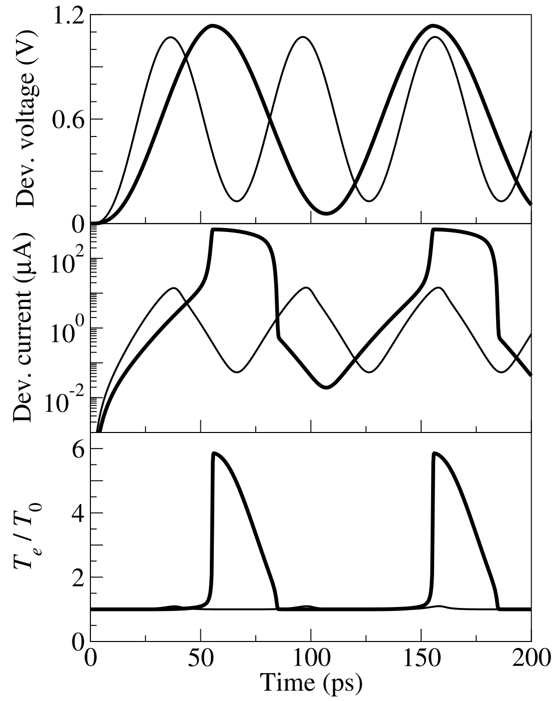

Fig. 3. Voltage drop (upper graphs), current response (center graphs), and electron temperature (lower graphs) of the Ovonic device in the circuit of Fig. 1, subjected to a voltage of period $T = 60$ ps (thin curve) and $T = 100$ ps (thick curve). See also Fig. 2.

The curves in Fig. 2 show the current response of the Ovonic device to an applied voltage of the form $V(t) = (V_0/2)\,[1 - \cos(2\,\pi\,t/T)]$, with $V_0 = 1.2$ V, for different values of the period T. The latter ranges from 10 ps to 10 ns. The device parameters are taken from experiments [8]: $R_L = 50\ \Omega$, $C = 150$ fF (hence $\tau_C = 7.5$ ps); moreover, we assumed

$\tau_T = 0.15$ ps, $\tau_n = 0.1$ ps. Under these bias conditions (note that the limits of V are 0 and V_0) the Ovonic device is voltage driven, and the working point oscillates between the lower and upper branches of the static $I(V)$ curve; no internal oscillations set in. Furthermore, for the case in hand, the characteristic time associated to the parasitic elements of the circuit, $\tau_C = R_L C$, turns out to be much larger than the relaxation times controlling the internal dynamics of the device; due to this, the time needed to charge/discharge the parasitic capacitance prevails over the internal dynamics.

Fig. 3 shows the voltage and current across the device, and the corresponding band-electron temperature, as functions of time for two periods among those used in Fig. 2. As apparent in the latter figure, the switching event sets in for $T = 100$ ps; in the $T = 60$ ps case, in contrast, no switching event occurs. Also, the $I(V)$ curve corresponding to $T = 60$ ps barely reaches the threshold voltage, then reverts onto itself. This outcome may qualitatively be ascribed to the shunting effect of capacitor C: such an effect increases with frequency and, as a consequence, the voltage drop across R_L is larger at $T = 60$ ps than in the $T = 100$ ps case. The different response is due to the interplay between the charging/discharging time of the parasitic capacitor and the characteristic times of the internal dynamics: when $T = 60$ ps, the field exceeds the threshold values for a relatively short time, and the corresponding temperature (lowest box of Fig. 3) is insufficient to trigger a switching event. The opposite happens when $T = 100$ ps.

When the period T of the applied bias is large, i.e., the device voltage changes little during a time of the order of τ_C, the current through the Ovonic device follows the static $I(V)$ curve and the voltages corresponding to the switching events coincide with the threshold and holding voltages of the latter (see, e.g., the $T = 10$ ns curve in Fig. 2). Switching events may also occur at shorter periods, provided the applied voltage is such that the capacitor is charged to a voltage larger than the static threshold voltage for a time long enough to produce carrier heating. In this situation, the delay due to the internal dynamics of the material shifts the switching voltage to higher values and the holding voltage to lower values ($T = 100$ ps curve in Fig. 2).

As noted above, no switching events occur when the period of the applied voltage becomes shorter ($T = 60$ ps and $T = 10$ ps curves in Fig. 2 for the case considered here). The qualitative analysis given earlier would be exact if the circuit were linear; in the present case, as the non-linearity of the Ovonic device introduces harmonics in addition to the fundamental frequency of the applied bias, the qualitative analysis must be corroborated by numerical results. The non-linear behavior of the device is evident in the current's waveform (center graphs of Fig. 3); besides that, the amplitude of the device voltage and, on a much larger scale, of the device current, decreases when the applied voltage's period decreases. This confirms the qualitative analysis carried out earlier, and reflects into the behavior of the band-electron temperature T_e shown in the lower graphs of the figure. In the $T = 60$ ps case the Ovonic material, still oscillating, remains in the lower branch of the $I(V)$ curve, and T_e keeps close to its equilibrium values.

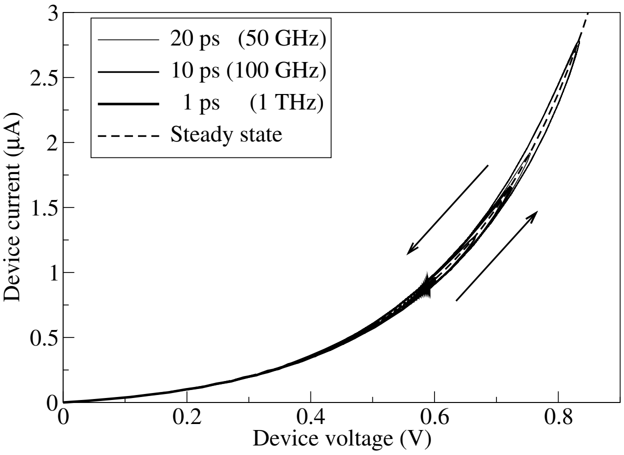

Fig. 4. Current response of the Ovonic device in the circuit of Fig. 1 subjected to an external voltage whose period T is comparable with, or shorter than, the internal-dynamics time.

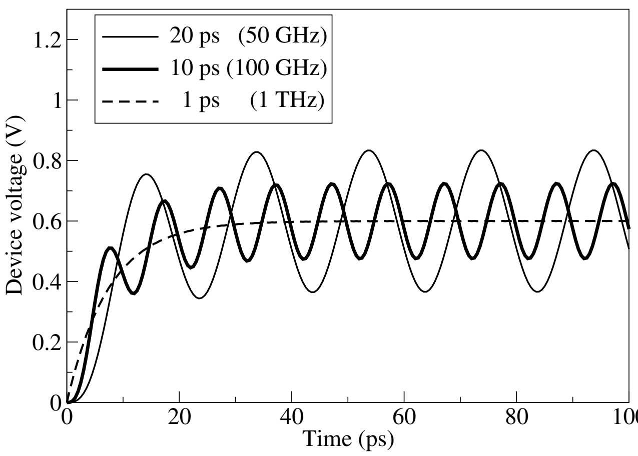

Fig. 5. Voltage across the Ovonic device, as a function of time, in the same conditions as those of Fig. 4. For the periods 1, 10, 20 ps used in the simulations, the Ovonic device never reaches the upper branch of the $I(V)$ curve during the time evolution.

At even higher frequencies of the applied voltage, the capacitance damps the response of the Ovonic material, progressively reducing the amplitude of its voltage oscillations around the bias average value, as shown in Figs. 4 and 5.

IV. Current-Driven Operation

In this section we consider the case where the bias voltage is applied through a very large series resistance, in such a way that the Ovonic device is essentially current driven. Besides using the same relaxation times as those reported in Sect. III, here we assume $R_L = 100$ kΩ, $R_S = 1$ kΩ, and different values for the capacitance C. The applied voltage has the same form as in Sect. III, with $V_0 = 10$ V and $T = 1$ ns. Of particular interest are the cases where the upper working

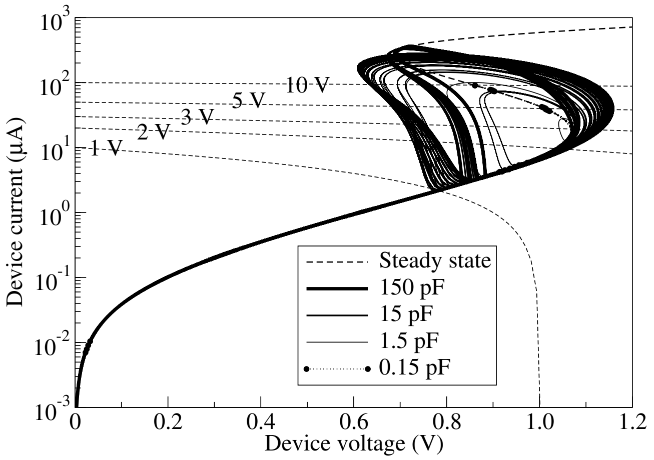

Fig. 6. $I(V)$ response of the Ovonic device at different circuit capacitance C. The short-dashed lines are the load lines for the values instantaneously reached by the bias during the oscillation. The working point never reaches the upper branch of the static $I(V)$ curve.

point of the device, during its oscillations, reaches the region of the static $I(V)$ curve where the differential resistance is negative (Fig. 6). The frequency of the applied voltage is small enough to allow for the setting up of the Ovonic oscillations, evidenced also in static conditions [11]. A stability analysis in the neighborhood of the working point, i.e., after linearizing the equations, was presented in [13]; here, a full large-signal analysis is tackled.

Fig. 7 shows the time variation of the Ovonic potential and current at different values of the capacitance, ranging from 150 to 0.15 fF. As expected, the frequency of the intrinsic oscillations increases as the capacitance decreases; when the capacitance decreases even further, the working point becomes stable and the oscillations extinguish (dashed curves in the upper and lower graphs of Figs. 7, corresponding to $C = 0.15$ fF).

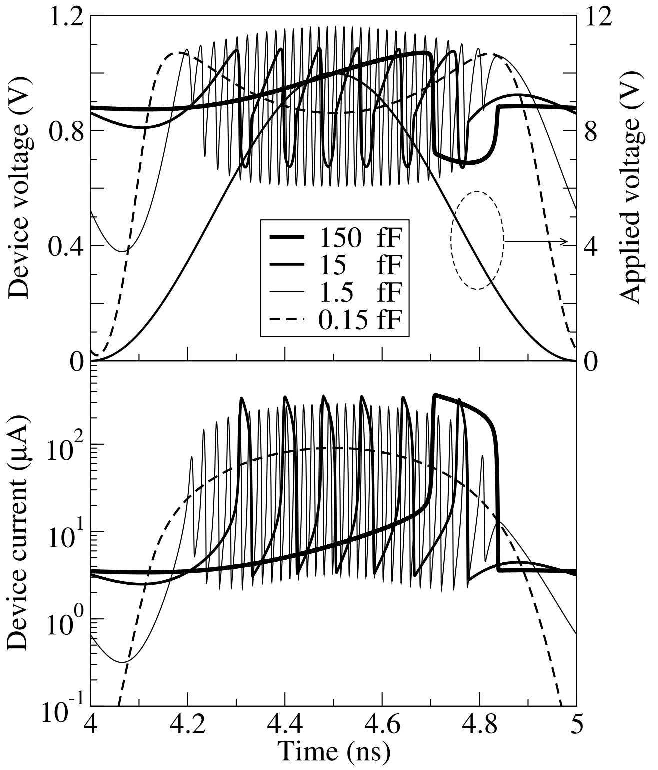

Fig. 7. Device voltage (upper graphs) and current (lower graphs) as functions of time for an applied oscillating voltage with $V_0 = 10$ V and $T = 1$ ns, at different values of the capacitance C. Here $R_L = 100$ kΩ and $R_S = 1$ kΩ. The working point of the Ovonic device never reaches the upper branch of the static $I(V)$ curve. The applied voltage is shown in the upper graphs (right scale).

V. Conclusions

In this paper, the model of [10], [11] has been used to identify different oscillating features of Ovonic Threshold-Switch devices by varying the details of the external bias and circuit elements, with the purpose of speculating about their influence on the performance of chalcogenide-based electronic products embedded into new-generation memory architectures. With respect to previous approaches, here the analysis has been extended to the case of an oscillating applied bias and to the large-signal case.

The outcome of the simulations shows how the features of the characteristic curves depend, besides the external bias, on the interplay between the material's intrinsic times and the unavoidable parasitic elements of the circuit. In the current-driven operation, either stable or oscillating solutions are found according to the load-line dynamics and the value of the parasitic capacitance. The results reveal the high-frequency oscillation potency of Ovonic materials, which can be exploited in the design of selector devices for two-terminal Non-Volatile Memories.

References

[1] Ovshinsky S R, 1968. *Phys. Rev. Lett.* **21**, 1450.
[2] Adler D, 1973. *J. Vac. Sci. Technol.* **10**, 728.
[3] Adler D, Shur M S, Silver M, Ovshinsky S R, 1980. *J. Appl. Phys.* **51**, 3289.
[4] Nardone M, Karpov V G, Jackson D C S, Karpov I V, 2009. *Appl. Phys. Lett.* **94**, 103509.
[5] Simon M, Nardone M, Karpov V G, Karpov I V, 2010. *J. Appl. Phys.* **108**, 064514.
[6] Ielmini D, 2008, *Phys. Rev. B* **78**, 035308.
[7] Piccinini E, Cappelli A, Buscemi F, Brunetti R, Ielmini D, Rudan M, and Jacoboni C, 2012. *J. Appl. Phys.* **112**, 083722.
[8] Wimmer M and Salinga M, 2014. *New J. Phys.* **16**, 113044.
[9] Lavizzari S, Ielmini D, and Lacaita A L, 2010. *IEEE Trans. Electron. Dev.* **57**, 1838.
[10] Buscemi F, Piccinini E, Brunetti R, Rudan M, and Jacoboni C, 2014. *Appl. Phys. Lett.* **104**, 262106.
[11] Piccinini E, Buscemi F, Rudan M, Brunetti R, and Jacoboni C, 2015. *Proc. EDISON'19, J. Phys. Conf. Series* **647**, 012021.
[12] Anbarasu M, Wimmer M, Bruns G, Salinga M, and Wuttig M, 2012. *J. Appl. Phys.* **100**, 143505.
[13] Rudan M, Piccinini E, Buscemi F, Brunetti R, 2015. *Proc. EUROSOI-IULIS* DOI 10.1109/ULIS.2015.7063838, 321–324.